ADVANCES IN ATMOSPHERIC SCIENCES, VOL. 38, FEBRUARY 2021, 296–306

• **Data Description Article** •

CAS-ESM2.0 Model Datasets for the CMIP6 Flux-Anomaly-Forced Model Intercomparison Project (FAFMIP)

Jiangbo JIN[1,2], He ZHANG[1], Xiao DONG[*1], Hailong LIU[3,4], Minghua ZHANG[1], Xin GAO[1], Juanxiong HE[1], Zhaoyang CHAI[1], Qingcun ZENG[1], Guangqing ZHOU[5], Zhaohui LIN[1], Yi YU[2], Pengfei LIN[3], Ruxu LIAN[1], Yongqiang YU[3,4], Mirong SONG[3], and Dongling ZHANG[1]

[1]*International Center for Climate and Environment Sciences*, *Institute of Atmospheric Physics*, *Chinese Academy of Sciences*, *Beijing* 100029, *China*

[2]*State Key Laboratory of Satellite Ocean Environment Dynamics*, *Second Institute of Oceanography*, *Ministry of Natural Resources*, *Hangzhou* 310012, *China*

[3]*State Key Laboratory of Numerical Modeling for Atmospheric Sciences and Geophysical Fluid Dynamics*, *Institute of Atmospheric Physics*, *Chinese Academy of Sciences*, *Beijing* 100029, *China*

[4]*College of Earth and Planetary Sciences*, *University of Chinese Academy of Sciences*, *Beijing* 100049, *China*

[5]*Institute of Atmospheric Physics*, *Chinese Academy of Sciences*, *Beijing* 100029, *China*

(Received 17 June 2020; revised 15 September 2020; accepted 29 October 2020)

ABSTRACT

The second version of the Chinese Academy of Sciences Earth System Model (CAS-ESM2.0) is participating in the Flux-Anomaly-Forced Model Intercomparison Project (FAFMIP) experiments in phase 6 of the Coupled Model Intercomparison Project (CMIP6). The purpose of FAFMIP is to understand and reduce the uncertainty of ocean climate changes in response to increased CO_2 forcing in atmosphere-ocean general circulation models (AOGCMs), including the simulations of ocean heat content (OHC) change, ocean circulation change, and sea level rise due to thermal expansion. FAFMIP experiments (including faf-heat, faf-stress, faf-water, faf-all, faf-passiveheat, faf-heat-NA50pct and faf-heat-NA0pct) have been conducted. All of the experiments were integrated over a 70-year period and the corresponding data have been uploaded to the Earth System Grid Federation data server for CMIP6 users to download. This paper describes the experimental design and model datasets and evaluates the preliminary results of CAS-ESM2.0 simulations of ocean climate changes in the FAFMIP experiments. The simulations of the changes in global ocean temperature, Atlantic Meridional Overturning Circulation (AMOC), OHC, and dynamic sea level (DSL), are all reasonably reproduced.

Key words: CAS-ESM2.0, CMIP6, FAFMIP, AMOC, ocean heat uptake, dynamic sea level change

Citation: Jin, J. B., and Coauthors, 2021: CAS-ESM2.0 Model Datasets for the CMIP6 Flux-Anomaly-Forced Model Intercomparison Project (FAFMIP). *Adv. Atmos. Sci.*, **38**(2), 296–306, https://doi.org/10.1007/s00376-020-0188-2.

1. Background

Currently, climate models exhibit large spread in their future projections of global climate. For instance, the coupled climate models of phase 5 of the Coupled Model Intercomparison Project (CMIP5) project a global mean sea level rise (SLR) of 0.32–0.63 m by 2081–2100 under the RCP4.5 scenario (Yin, 2012; IPCC, 2013), and the thermosteric contribution due to seawater expansion can be up to 30% of the global mean SLR and up to 100% in the North Atlantic region (Gregory et al., 2016). The spread of ocean climate changes may be associated with the spread of the surface flux perturbation responses to increased atmospheric CO_2 concentrations (Bouttes and Gregory, 2014). However, the spatial patterns and magnitudes of the sea surface flux perturbations are largely model-dependent, which makes it complicated and difficult to directly compare ocean responses in coupled models. Therefore, to understand the ocean responses to increased CO_2 levels and reduce the uncertainty of ocean state estimations, a flux-anomaly-forced model intercomparison project (FAFMIP), one of 23 Model Intercomparison Projects (MIPs) in CMIP6 (Eyring et al., 2016), has been proposed to compare the different model responses to the same prescribed surface flux perturbations (Gregory et al., 2016). According to Gregory et al. (2016),

* Corresponding author: Xiao DONG
Email: dongxiao@mail.iap.ac.cn

around ten modeling groups plan to participate in FAFMIP. At the time of this report, FAFMIP experiment outputs from nine models are available on the Earth System Grid Federation (ESGF) data server for CMIP6.

In China, thirteen models from nine institutes or universities in mainland China and Taiwan are participating in CMIP6 (Zhou et al., 2019), and are using thirteen different models. Among these models, CAS-ESM2.0 is an earth system model (ESM) from the Institute of Atmospheric Physics, Chinese Academy of Sciences (IAP/CAS), which has a long history for the development of climate models. Since the 1980s, scientists at IAP/CAS have been devoted to developing climate models that include an atmospheric general circulation model (AGCM), ocean general circulation model (OGCM), and land surface model (LSM) (Zhang and Zeng, 1988; Zeng et al., 1989; Dai and Zeng, 1997), which have been used for short-term climate predictions in China and have participated in each phase of CMIP since the 1990s (Zhou et al., 2020). CAS-ESM2.0 is the successor to CAS-ESM1.0, which was released to the public in 2015. Compared to CAS-ESM1.0, CAS-ESM2.0 considerably modified codes and parameterization schemes in most components, as well as substantially improved performance in its climate simulations (Zhang et al., 2020; Zhou et al., 2020). The FAFMIP experiments were completed using CAS-ESM2.0 by closely following the standard protocol of Gregory et al. (2016); the corresponding data have been uploaded to the ESGF data server for CMIP6 users to download and can be found at https://esgf-node.llnl.gov/projects/cmip6/.

The purpose of this paper is to present the preliminary results of CAS-ESM2.0 for simulations of ocean changes in FAFMIP experiments for users of the CMIP6 datasets. The remainder of the paper is structured as follows: Section 2 describes the model and experiments; section 3 provides a basic technical validation of the CAS-ESM2.0 experiments; and sections 4 and 5 offer usage notes and a summary, respectively.

2. Model and experimental design

2.1. *Model*

CAS-ESM2.0 is a fully coupled ESM that was developed at IAP/CAS. It is based on IAP AGCM version 5 and is derived from the LASG/IAP Climate System Ocean Model (LICOM2), Beijing Normal University/IAP Common Land Model (CoLM), Los Alamos Sea Ice Model (CICE version 4), and the Weather Research and Forecasting (WRF) model. The infrastructure of CESM Coupler 7 is adopted to ensure that the components are coupled together. Additional components in CAS-ESM2.0 include the IAP Vegetation Dynamics Model and IAP fire model, which are embedded within the land model; the IAP ocean biogeochemistry model, which is embedded within the ocean model; an atmospheric aerosol and chemistry model; and various emission models. However, the climate components, which include atmosphere, ocean, land and sea ice, are the main focus in the FAFMIP experiments. A schematic diagram of the CAS-ESM2.0 framework is shown in Fig. 1.

The atmospheric component of CAS-ESM2.0 is IAP AGCM5.0, which is the fifth-generation AGCM developed by IAP. The IAP AGCM is a global gridpoint model that uses the finite-difference scheme with terrain-following for the σ-coordinate. The horizontal resolution of IAP AGCM5 is approximately 1.4° latitude × 1.4° longitude and has 35 vertical levels with a model top at 2.2 hPa. The physical parameterizations in IAP AGCM5 have been largely updated and include new convection and cloud schemes and many modifications that were made to other parameterization schemes compared to its previous version, IAP AGCM4.1, in which the physical parameterizations were mostly taken from CAM5 (Zhang et al., 2020).

The OGCM in CAS-ESM2.0 is based on LICOM2.0 (Liu et al., 2012). The model domain is located between 78.5°S and 87.5°N with a 1° zonal resolution. The meridional resolution is refined to 0.5° between 10°S and 10°N

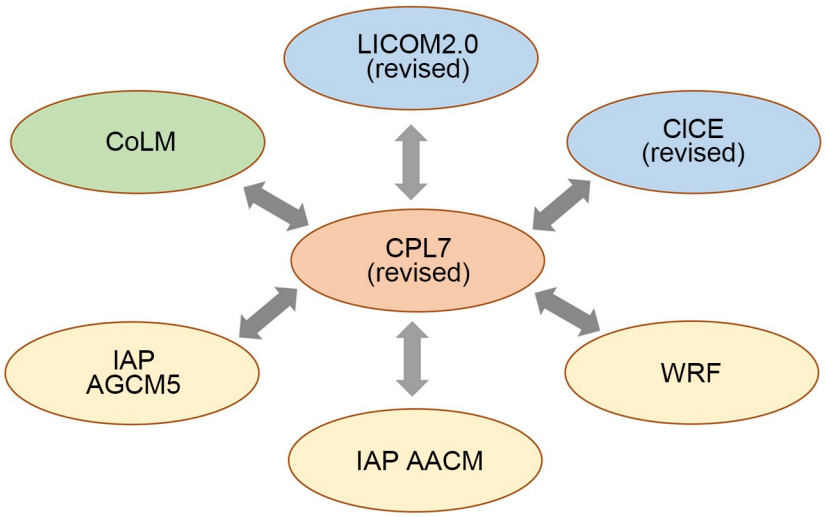

Fig. 1. Schematic diagram of the CAS-ESM2.0 framework.

and is increased gradually from 0.5° to 1° between 10° and 20°. There are 30 levels in the vertical direction with 10 m per layer in the upper 150 m. Based on the original version of LICOM2.0, key modifications have been made: (1) a new sea surface salinity boundary condition was introduced that is based on the physical process of air–sea flux exchange at the actual sea–air interface (Jin et al., 2017); (2) intra-daily air–sea interactions are resolved by coupling the atmospheric and oceanic model components once every 2 h; and (3) a new formulation of the turbulent air–sea fluxes (Fairall et al., 2003) was introduced. The ocean component of CAS-ESM2.0 has also participated the Ocean Model Intercomparison Project Phase 1 (OMIP1) experiments for CMIP6 (Dong et al., 2020).

The sea-ice model is the improved Los Alamos Sea Ice Model (version 4.0) (Hunke and Lipscomb, 2008) and uses the same grid as the oceanic model. This model solves the dynamic and thermodynamic equations for five ice-thickness categories, with one snow layer and four ice layers. For the dynamic component, we use elastic–viscous–plastic rheology (Hunke and Dukowicz 1997), the mechanical redistribution scheme (Lipscomb et al., 2007), and the incremental remapping advection scheme (Lipscomb and Hunke, 2004). For the thermodynamic component, we use parameterization with a more realistic sea-ice salinity budget (Liu, 2010) and an improved CCSM3 radiation scheme for albedo and radiative fluxes at the sea-ice surface by incorporating an explicit melt pond and its impact on the albedo.

The land component of CAS-ESM2.0 is CoLM (Dai et al., 2003). The initial version of CoLM was adopted as the Community Land Model (CLM) for use with the Community Climate System Model (CCSM; Collins et al., 2006), which was later adopted as the land component for the Beijing Normal University Earth System Model (BNU-ESM; Ji et al., 2014). The improved version of CoLM has been adopted in CAS-ESM2, e.g., an improved two-stream approximation model of radiation transfer of the canopy, a photosynthesis–stomatal conductance model for sunlit and shaded leaves and for simultaneous transfer of CO_2 and water vapor into and out of the leaves, and the embedded IAP Dynamic Global Vegetation Model (IAP-DGVM) (e.g., Dai et al., 2004; Zeng et al., 2014).

2.2. *Experimental design*

The FAFMIP experiments are flux-anomaly-forced experiments and have been conducted using CAS-ESM2.0. A detailed description of the experimental design of the FAFMIP experiments was supplied by Gregory et al. (2016). FAFMIP presents the prescribed surface flux perturbations of wind stress, heat and fresh water for the doubled CO_2 concentrations (Figs. 2a–c), which are derived from the ensemble mean differences between years 61–80 of 13 CMIP5 CGCM 1pctCO_2 experiments and all years of piControl control simulations and held seasonal cycles. Seven experiments (namely, faf-stress, faf-heat, faf-water, faf-heat-

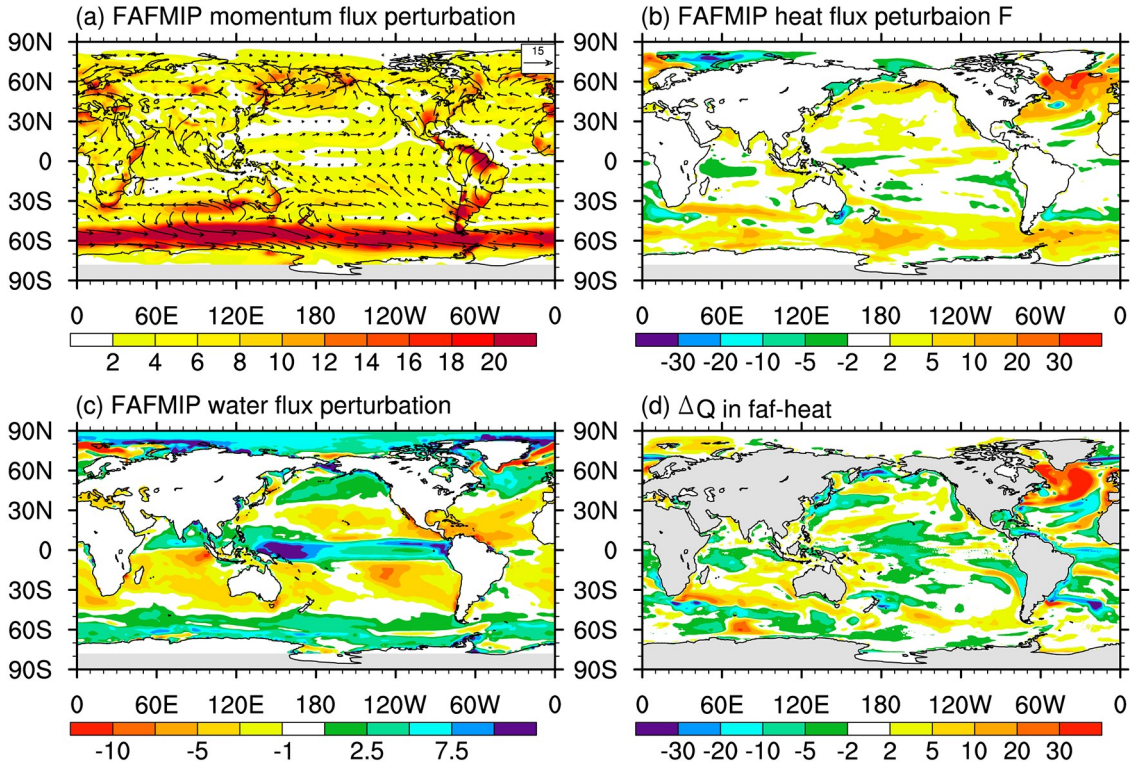

Fig. 2. Spatial patterns of the surface flux perturbations of (a) momentum (units: 10^{-3} Pa; colors indicate magnitude of the vector, arrows indicate direction), (b) heat (units: W m^{-2}), and (c) water (units: 10^{-6} kg m^{-2} s^{-1}) as added atmospheric forcing in FAFMIP experiments. (d) Spatial pattern of change in the surface heat flux into seawater in the time mean of the final decade of the faf-heat experiment relative to the control (units: W m^{-2}).

NA50pct, faf-all, faf-passiveheat, and faf-heat-NA0pct) were conducted using CAS-ESM2.0. Among the experiments, the former four experiments are Tier1, while the latter three are Tier2. The corresponding experimental designs are briefly described as follows:

(1) In the faf-stress experiment, a perturbation occurs in the surface eastward (zonal) and northward (meridional) momentum fluxes, i.e., wind stress is added to the momentum balance of the seawater surface. Figure 2a shows the annual mean surface momentum flux perturbations supplied by FAFMIP. The prominent feature is the westerly wind stress in the Southern Ocean, for which the largest positive change exceeds 0.02 Pa.

(2) In the faf-heat experiment, a perturbation of the heat flux is imposed on the ocean water surface. Figure 2b shows the heat flux perturbation forcing in the FAFMIP experiment. Larger positive anomalies occur in the mid–high-latitude North Atlantic Ocean and in the Southern Ocean. To eliminate the strong negative feedback between the surface heat flux and SST and to maximize the effect of the prescribed surface heat flux perturbation, we adopted the tracer approach method B that was recommended by FAFMIP. This method divides the temperature change and ocean heat uptake (OHU) into added (T_a', mainly due to the prescribed added heat flux) and redistributive (T_r', mainly due to the change in ocean circulation) components in the related heat flux perturbation experiments, and the passive heat tracer T_r' is introduced and used to calculate the surface heat flux instead of SST, which does not feel heat flux perturbations and affects ocean water density.

(3) In the faf-water experiment, a perturbation of the freshwater flux is added to the sea water surface. Figure 2c shows the annual mean surface water flux perturbation. The pattern is dominated by precipitation changes and the positive center is located in the western equatorial Pacific and in the midlatitudes of the two hemispheres. In contrast, negative water flux occurs in the subtropics.

(4) The design of the faf-heat-NA50pct experiment is exactly the same as that of the faf-heat experiment except that within a portion of the North Atlantic Ocean, the heat flux perturbation is multiplied by 0.5, as was proposed at the FAFMIP meeting in April 2019. The purpose of the experiment is to produce an Atlantic Meridional Overturning Circulation (AMOC) weakening that is similar to that in 1pctCO2, whereas the original faf-heat experiment provides greater weakening because of the redistribution feedback.

(5) In the faf-all experiment, the surface flux perturbations of momentum, heat and freshwater are simultaneously imposed on seawater. Method B is also applied to compute the surface flux, which is the same method as in the faf-heat experiment. The experiment is used to quantify the nonlinearities of the effects of the three perturbations.

(6) In the faf-passiveheat experiment, the heat flux perturbation is applied instead to the passive tracer T_a initialized to zero, which can be used to diagnose the effect of added heat on ocean temperatures due to ocean circulation changes through a comparison of faf-passiveheat with faf-heat. The experiment is equivalent to the piControl experiment. The results of this experiment are used as a control experiment in this paper.

(7) The faf-heat-NA0pct experiment is similar to faf-heat-NA50pct but with a zero perturbation in the North Atlantic region, as was also proposed at the FAFMIP meeting in April 2019.

It is noteworthy that all perturbations are imposed on the seawater surface and do not directly affect the sea ice, to maintain the preindustrial state of the sea ice. The initial conditions of all experiments are the same, and are derived from the end of a 300-year spin up of the piControl experiment of CAS-ESM2.0. Further details of the implementation of each of the experiments can be found at the following websites: http://www.fafmip.org and http://www.fafmip.org/design_apr19.html.

3. Technical validation

Surface heat flux perturbation plays a dominant role in the weakening of the AMOC and increases the OHU and SLR among the surface flux perturbations (Rahmstorf and Ganopolski, 1999; Gregory et al., 2005; Bouttes and Gregory, 2014; Gregory et al., 2016). Therefore, minimization of the effect of the redistributed heat flux change ΔQ due to circulation changes is very important in the faf-heat and faf-all experiments. Figure 2d shows the change in the surface ΔQ of the faf-heat experiment relative to that of the control. The spatial pattern is consistent with the multimodel mean results shown in Gregory et al. (2016). The most significant positive change is observed in the North Atlantic and a negative flux change can be observed in the equatorial Pacific and Atlantic, western boundary in the North Pacific and around the Aleutian Islands, and along the western and eastern coasts of the South American continent. The global ocean area mean ΔQ in the final decade is 0.15 W m^{-2}, which is slightly greater than the multimodel mean result (0.07 W m^{-2}) presented in Gregory et al. (2016). The global ocean area mean heat flux perturbation is 1.86 W m^{-2}, and thus 108% of the heat flux perturbation is added to the ocean, which results in a greater increase in the ocean temperature than that in faf-passiveheat (Fig. 3c).

3.1. *Time series of changes*

Figure 3 shows the time series of several key metrics in the experiments following Gregory et al. (2016), which include the global mean surface air temperature change (Fig. 3a), net surface heat flux change (Fig. 3b), ocean volume mean temperature change (Fig. 3c), and maximum AMOC transport change (Fig. 3d). From the results of the surface air temperature change, faf-stress varies up and down slightly above the zero line, whereas the faf-heat, faf-water and faf-all experiments all show surface cooling with a magnitude within −0.5°C. Our results are similar to the model performance in Gregory et al. (2016, top row of their Fig. 5), especially regarding the consistency of the results simu-

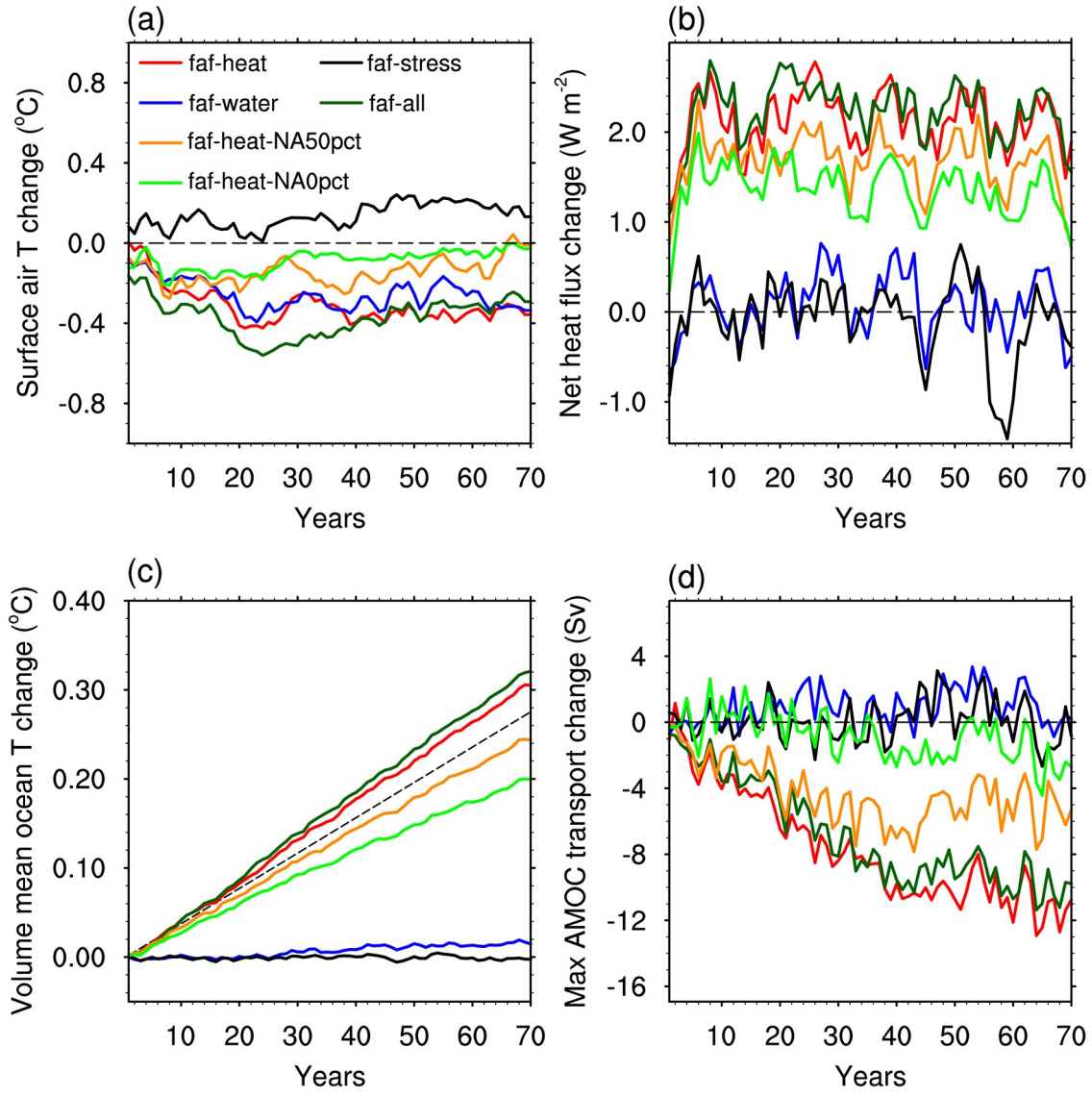

Fig. 3. Annual mean time series of the (a) surface air temperature change (units: °C), (b) net heat flux change (units: W m^{-2}), (c) volume mean ocean temperature change (units: °C), and (d) maximum transport change of the AMOC (units: Sv), in six experiments: faf-heat (red line), faf-stress (black line), faf-water (blue line), faf-all (dark green line), faf-heat-NA50pct (orange line) and faf-heat-NA0pct (green line). The dashed black line indicates the faf-passiveheat experiment.

lated by GFDL-ESM2M. The magnitudes of air temperature change in faf-heat-NA50pct and faf-heat-NA0pct are notably smaller compared to those in faf-heat due to the reduced heat flux perturbation in the North Atlantic region. These results show a decrease in the surface air temperature change in the faf-heat and faf-all experiments, which is mainly associated with the surface heat flux perturbation, especially for the North Atlantic region. The imposed heat flux perturbation in the North Atlantic region could reduce heat transport by AMOC in the heat flux perturbation experiments, which would further induce cooling of air temperatures in the North Atlantic region and for similar-latitude regions of Eurasia and North America (Stouffer et al., 2006). In faf-water, cooling of the surface air temperature is mainly due to the suppression of upward heat transport caused by fresher surface salinity (Gregory et al. 2016).

As shown in Fig. 3b, the net surface heat flux change is positive (~2 W m^{-2}) in faf-heat and faf-all, whereas in faf-stress and faf-water the net surface heat flux change oscillates near the zero line, which indicates that the net heat flux in faf-all is mainly attributable to the surface heat flux change. In our experiments, the global mean heat flux over the last 10 years is 2.01 (2.15) W m^{-2} in faf-heat (faf-all), and the global mean prescribed heat flux perturbations in faf-heat and faf-all are 1.86 W m^{-2}. Compared with faf-heat and faf-all, the positive heat flux changes in faf-heat-NA50pct and faf-heat-NA0pct are suppressed due to the experimental designs, and the global mean surface heat flux changes in the final decade of the two experiments are 1.55 W m^{-2} and 1.28 W m^{-2}, respectively.

In Fig. 3c, the ocean volume mean temperatures increase continuously in the faf-heat and faf-all experiments; however, the faf-water and faf-stress experiments both show minor changes and the faf-water experiment has a slightly larger magnitude of increase than the faf-stress experiment. This feature is highly consistent with the results of Gregory et al. (2016, second row of their Fig. 5). At the end of the 70th year of integration, the temperature change in faf-heat (faf-all) is approximately 0.30°C (0.32°C), with the same magnitude as MPI-ESM-LR in Gregory et al. (2016), which is slightly larger than the T_a (0.28°C) in faf-passiveheat forced only by the prescribed heat flux perturbation. The larger increases in temperature changes in faf-heat and faf-all compared to T_a in faf-passiveheat are due to the warming effects of ΔQ (Fig. 3a). Similar to the air temperature and surface heat flux changes, the variations of ocean volume-mean temperatures in the faf-heat-NA50pct and faf-heat-NA0pct experiments are consistent with those in the faf-heat and faf-all experiments but with reduced magnitudes. The positive ocean volume-mean temperature anomalies at the end of the integrated 70th year reach 0.24°C and 0.20°C in faf-heat-NA50pct and faf-heat-NA0pct, respectively.

The strength of AMOC is decreased in the faf-heat and faf-all experiments with similar magnitudes (approximately −10 Sv) (Fig. 3d). Our results falls in the uncertainty range (e.g., 6–12 Sv) of the models in Gregory et al. (2016, third row of their Fig. 5), with a magnitude similar to CanESM2. In the first 30 years in the faf-heat-NA50pct experiment, the reduction of AMOC is nearly consistent with those in the faf-all and faf-heat experiments. After 30 years, the difference between faf-heat-NA50pct and faf-heat/faf-all increases with an ultimate reduction in AMOC to approximately half of that in the faf-all and faf-heat experiments at the end of the 70th year. In the faf-heat-NA0pct experiment, the AMOC change is largely suppressed (within −4 Sv) due to the absence of the surface heat flux perturbation imposed in the North Atlantic region. Compared with the faf-all and faf-heat experiments, no significant AMOC changes occur in the faf-stress and faf-water experiments (Figs. 3c and d). These time series of the global mean variables further demonstrate that the surface heat flux perturbation plays a dominant role in ocean climate change in response to CO_2 forcing among the surface flux perturbations.

3.2. *Spatial patterns of changes*

Figure 4 shows the zonal mean ocean temperature changes in the time means of the final decade of the FAFMIP experiments relative to the control experiment. In faf-heat, the warming is mainly located in the upper 1000 m over nearly the entire ocean (Fig. 4a), with the maximum magnitude of change exceeds 1°C to the north of 40°N and penetrates to a depth of 500 m. The cooling in faf-heat appears north of 60°N from 500 m to 2000 m and approximately 40°N from 2500 m to 3500 m. The warming in faf-heat is dominated by the added heat tracer T_a' due to the imposed surface flux perturbation (Fig. 4g), and the cooling mainly results from the redistributed heat tracer T_r' due to ocean circulation change, especially for the change in AMOC (Fig. 4h). The spatial patterns of zonal mean ocean temperature changes, the added heat tracer T_a', and the redistributed heat tracer T_r' in faf-heat, are highly consistent with the results of Gregory et al. (2016, third row in their Fig. 11). The spatial patterns of the zonal mean ocean temperature changes in faf-all are highly similar to those in faf-heat. The faf-water experiment contributes warming (approximately 0.2°C) in the Northern Hemisphere at depths of approximately 500–2000 m and cooling at depths of 0–500 m in the Southern Ocean (Fig. 4b); faf-stress exhibits a cooling pattern in most upper-ocean regions. The spatial patterns of the zonal mean temperatures in faf-heat-NA50pct and faf-heat-NA0pct are also similar to those in faf-heat, and the magnitude of warming north of 40°N from the surface to a depth of 500 m and cooling in the mid–high-latitude subsurface in both experiments are substantially reduced compared to those in faf-heat. This demonstrates the combined effects of the difference in the heat flux perturbation imposed in the North Atlantic region and the difference in the reduction of heat transport by AMOC.

Changes in ocean heat content (OHC) and dynamic sea level (DSL) are also important metrics for evaluating ocean climate change, which is an essential scientific issue that the community aims to resolve by conducting the FAFMIP experiments. We show the spatial patterns of the DSL and OHC changes in the time means of the final decade of the FAFMIP experiments in Fig. 5 and Fig. 6, respectively. The greatest local changes in DSL and in OHC occur in faf-heat among the surface flux perturbation experiments (Fig. 5 and Fig. 6). The most striking feature in faf-all is the three dipole patterns of DSL change: one is located in the North Atlantic (a positive change at approximately 40°N and a negative change southward); the second is located across the Antarctic Circumpolar Circulation (ACC, a positive change to the north and negative change to the south); and the last is over the North Pacific with an opposite dipole pattern of passive change in subtropical areas and a negative change to the north, which are highly similar to the model-mean results in Gregory et al. (2016, their Fig. 8). The North Atlantic dipole pattern is primarily due to the heat flux perturbation (Figs. 5a and d), which is consistent with a larger increase in OHC north of 40°N in the Atlantic Ocean in faf-heat and faf-all (Figs. 6a and d). Additionally, the water flux perturbation can partially reinforce the North Atlantic dipole due to the halosteric contribution because an increase in OHC occurs in most areas of the North Atlantic in faf-water (Fig. 6b), although the AMOC does not change substantially (Fig. 3b). The dipole pattern across the ACC results from the combined effects of the heat and wind stress perturbations and the water flux perturbations provide a counteracting contribution (Figs. 5b–d). The contributions of the heat, water and wind stress perturbations to the DSL changes across the ACC are mainly thermosteric instead of halosteric, as is inferred from the distributions of OHC

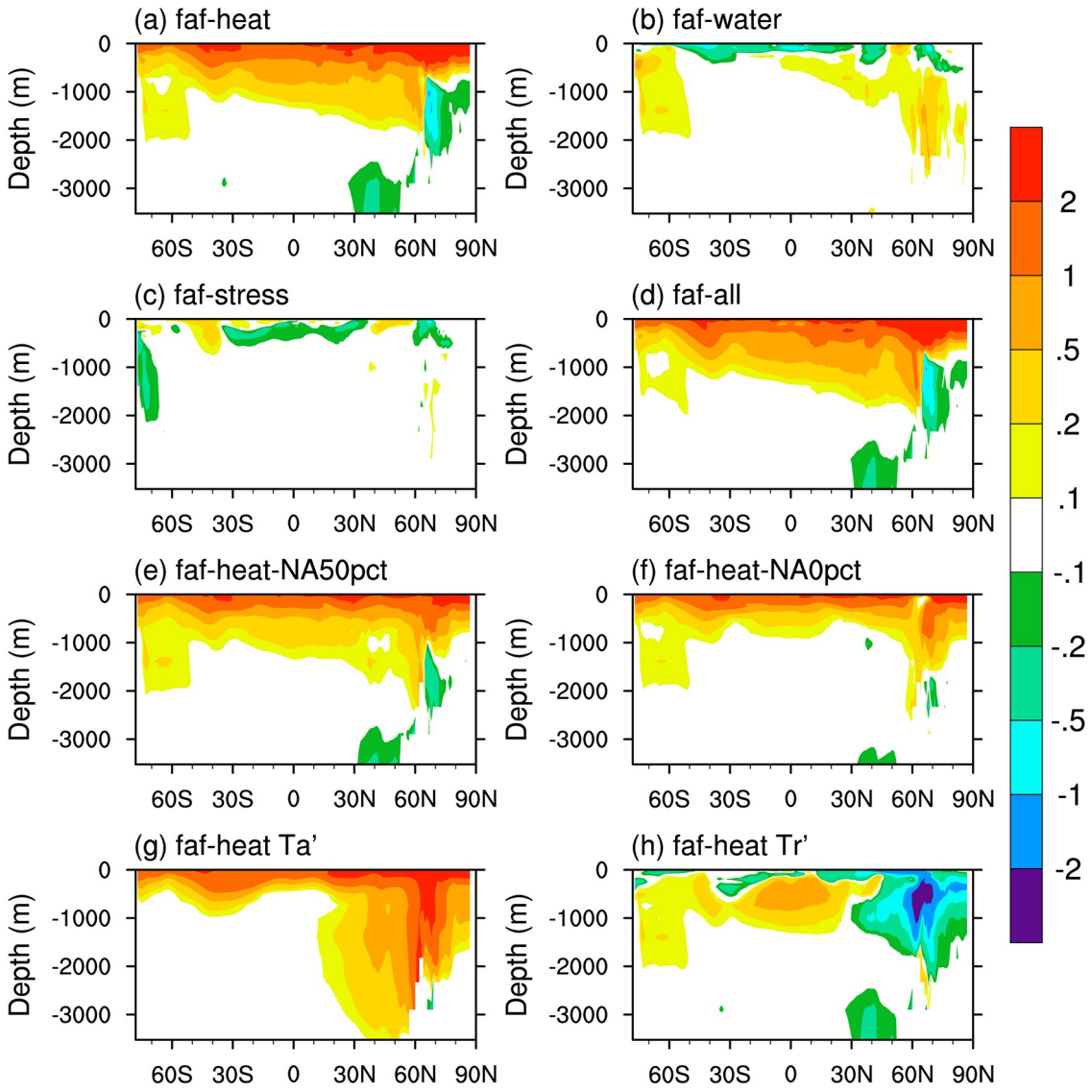

Fig. 4. Latitude–depth plots of the zonal mean ocean temperature change (units: °C) in the time mean of the final decade in FAFMIP minus that in the control experiment, in six experiments: (a) faf-heat, (b) faf-water, (c) faf-stress, (d) faf-all, (e) faf-heat-NA50pct, and (f) faf-heat-NA0pct. In addition, (g) and (h) represent added and redistributed portions in the faf-heat experiment, respectively.

change (Figs. 6a–d). The opposite dipole pattern over the North Pacific is due to the combined effects of surface heat flux and freshwater flux perturbations (Figs. 6a, b and d).

For the two new experiments (i.e., faf-heat-NA50pct and faf-heat-NA0pct), although the dipole pattern across the ACC still exists in faf-heat-NA50pct and faf-heat-NA0pct (Figs. 5e and f), the magnitude of the DSL change gradient across the ACC is significantly lower when compared with that of faf-heat, which is associated with the smaller increase in OHC (Figs. 6g and h). For the North Atlantic, the increase in OHC north of 40°N in faf-heat-NA50pct is greatly reduced compared with that in faf-heat, and faf-heat-NA0pct shows almost no increase in this region, which mainly results from the suppressed heat flux perturbation imposed in the North Atlantic in both experiments. The change in the North Atlantic dipole pattern in DSL in faf-heat-NA50pct is not obvious, and faf-heat-NA0pct exhibits an almost opposite dipole pattern.

The spatial patterns of the changes (including changes in the zonal mean temperature, OHC and DSL) in faf-all are mainly dominated by those in faf-heat. We further explore the added OHC change $\left(\int_0^{-H}\rho_0 c_p T_a' \mathrm{d}z\right)$ and redistributed OHC change $\left(\int_0^{-H}\rho_0 c_p T_r' \mathrm{d}z\right)$ of the OHC change in the faf-heat experiment, and the results are shown in Figs. 6 g and h, where ρ_0, c_p and H represent the sea water density, specific heat capacity and depth of the sea water, respectively. Similar to the zonal mean temperature change, the increased OHC in faf-heat is primarily determined by the added OHC change, especially for the Atlantic Ocean and Southern Ocean. It is noted that the redistributed OHC change is also important for determining the geographical pattern of the

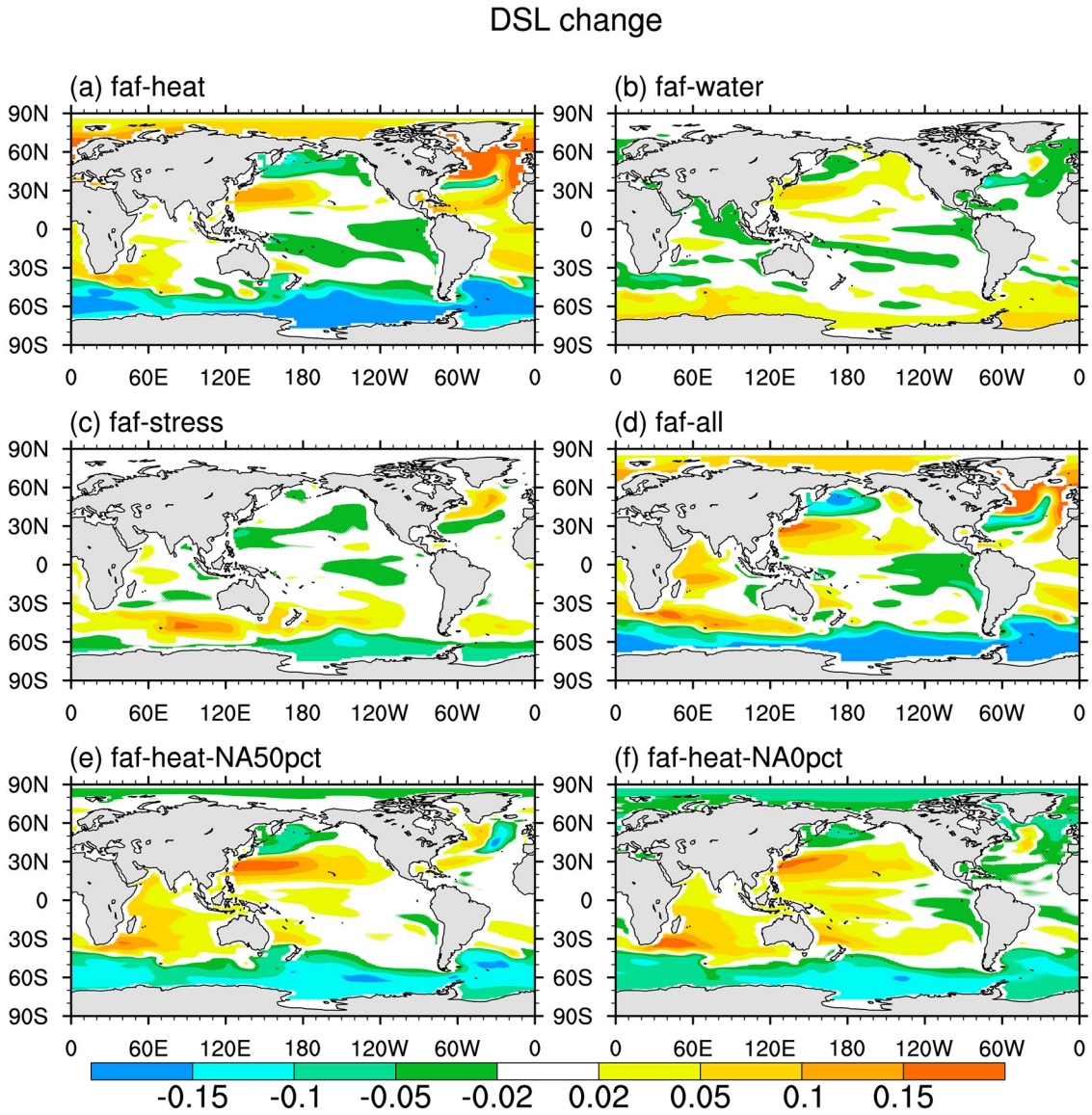

Fig. 5. Spatial patterns of the DSL change (units: m) averaged in the final decade relative to the control in six experiments: (a) faf-heat, (b) faf-water, (c) faf-stress, (d) faf-all, (e) faf-heat-NA50pct, and (f) faf-heat-NA0pct.

OHC change, such as in the North Atlantic, western boundary currents, and high latitudes.

Using the FAFMIP multimodel output datasets, further investigations can be performed to examine future ocean circulations and energy changes with increasing CO_2 levels.

4. Usage notes

The FAFMIP datasets, including those from the faf-all, faf-heat, faf-water, faf-stress, faf-passiveheat, faf-heat-NA50pct and faf-heat-NA0pct experiments, have been uploaded to the ESGF data server for users to download and can be found at https://esgf-nodes.llnl.gov/projects/cmip6/. The dataset format is the NetCDF (Network Common Data Form), version 4. The horizontal grid numbers of the model outputs are 360 and 196 in the zonal and meridional directions, respectively. The data have 30 vertical levels with 10 m per layer in the upper 150 m and the original horizontal resolutions and vertical levels are not changed on the ESGF nodes. The variables of Priority 1 for FAFMIP are shown in Table 1. The corresponding piControl data are also available from the same website.

5. Summary

The purpose of this paper is to introduce the FAFMIP experimental datasets in CMIP6 as simulated by CAS-ESM2.0 and to provide a brief evaluation of the model performances in this regard. Seven FAFMIP experiments (including faf-heat, faf-stress, faf-water, faf-all, faf-passiveheat, faf-heat-NA50pct and faf-heat-NA0pct) have been conducted using CAS-ESM2.0, with each experiment integrated over 70 years. As expected, the temporal evolutions of the global mean variables (including the changes in ocean temper-

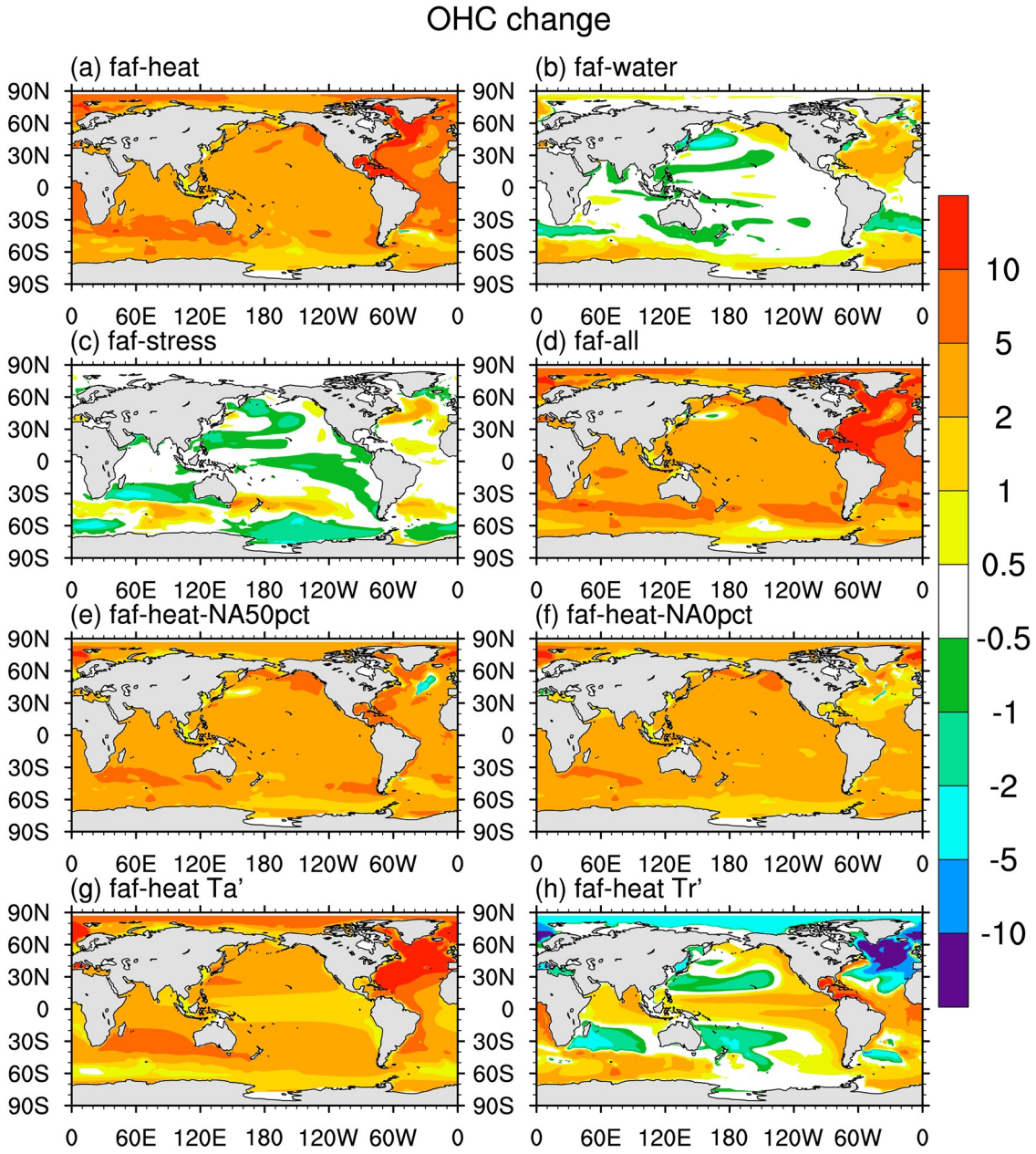

Fig. 6. Spatial patterns of the OHC change (units: GJ m^{-2}; vertical integral of the change in the tracer multiplied by the volumetric heat capacity) averaged in the final decade relative to the control in eight experiments. Experiments (a) to (f) is the same as in Fig. 5, while (g) and (h) are experiments that separate the added (T_a') and redistributive (T_r') components in the heat flux perturbation experiments. Detailed information of these experiments can refer to Section 2.2 (Experimental design).

ature, surface air temperature, surface heat flux, and AMOC) and the spatial patterns of ocean climate changes (including DSL and OHC changes) in CAS-ESM2.0 are highly consistent with the preliminary results of other models reported in Gregory et al. (2016).

As in many previous studies, surface heat flux perturbations play a dominant role in ocean climate changes (including DSL, AMOC and OHC changes) in response to CO_2 forcing among the surface flux perturbations. Heat flux and water flux perturbations cause the DSL dipole pattern in the North Atlantic, while the Southern Ocean features of DSL change are mainly caused by heat and wind stress perturbations, and water flux perturbations have a counteracting contribution. The AMOC decreases in response to surface heat flux perturbations and the wind stress and water flux perturbations have almost no effect on AMOC change. The two newly added experiments (i.e., faf-heat-NA50pct and faf-heat-NA0pct) greatly reduce the weakening of AMOC, and the dipole pattern of DSL in the North Atlantic is markedly different from those in faf-heat and faf-all. Therefore, the rationality of the two new experiments needs to be further investigated. For the OHC changes, the increased OHC in

Table 1. Information on the CAS-ESM2.0 uploaded variables for FAFMIP, including name, description and frequency.

Name	Description	Frequency
zos	sea surface height above geoid	monthly
zostoga	global average thermosteric sea level	monthly
thetao	sea water potential temperature	monthly
thetaoga	global average sea water potential temperature	monthly
so	sea water salinity	monthly
msftmz	ocean meridional overturning mass streamfunction	monthly
hfds	downward heat flux at sea water surface	monthly
pathetao	sea water additional potential temperature	monthly
prthetao	sea water redistributed potential temperature	monthly
opottempdiff	tendency of sea water potential temperature expressed as heat content due to parameterized dianeutral mixing	yearly
opottemppadvect	tendency of sea water potential temperature expressed as heat content due to parameterized eddy advection	yearly
opottemppmdiff	tendency of sea water potential temperature expressed as heat content due to parameterized mesoscale diffusion	yearly
opottemprmadvect	tendency of sea water potential temperature expressed as heat content due to residual mean advection	yearly
opottemptend	tendency of sea water potential temperature expressed as heat content	yearly
osaltdiff	tendency of sea water salinity expressed as salt content due to parameterized dianeutral mixing	yearly
osaltpadvect	tendency of sea water salinity expressed as salt content due to parameterized eddy advection	yearly
osaltpmdiff	tendency of sea water salinity expressed as salt content due to parameterized mesoscale diffusion	yearly
osaltrmadvect	tendency of sea water salinity expressed as salt content due to residual mean advection	yearly
osalttend	tendency of sea water salinity expressed as salt content	yearly

faf-heat is primarily determined by the added OHC change, especially for the Atlantic Ocean and Southern Ocean, and the redistributed OHC changes due to ocean circulation changes are also important for influencing the geographical patterns of OHC changes.

Based on the reasonable behaviors of the model results, further research can be performed to explore the changes in OHC, ocean circulation and sea level response to CO_2 forcing by using our model outputs along with other FAFMIP datasets. The FAFMIP experimental outputs can be compared with the 1pctCO2 experiments in CMIP6 to investigate the uncertainty of ocean responses to increasing CO_2 levels. Our experimental datasets have been uploaded to the CMIP6 website and all scientists and researchers are welcome to download and use the data. The results in this paper also serve as a basic reference of CAS-ESM2.0 performance for all users who are interested in the FAFMIP experiments and who might use our datasets.

Acknowledgements. This research was supported by the National Major Research High PerformanceComputing Program of China (Grant No. 2016YFB0200804), the National Natural Science Foundation of China (Grant Nos. 41706036, 41706028, 41975129 and 41630530), the open fund of State Key Laboratory of Satellite Ocean Environment Dynamics, Second Institute of Oceanography (Grant No. QNHX2017), and the National Key Scientific and Technological Infrastructure project entitled "Earth System Science Numerical Simulator Facility" (EarthLab) and key operation construction projects of Chongqing Meteorological Bureau- "Construction of chongqing short-term climate numerical prediction platform".

REFERENCES

Bouttes, N., and J. M. Gregory, 2014: Attribution of the spatial pattern of CO_2-forced sea level change to ocean surface flux changes. *Environmental Research Letters*, **9**, 034004, https://doi.org/10.1088/1748-9326/9/3/034004.

Collins, W. D., and Coauthors, 2006: The community climate system model version 3 (CCSM3). *J. Climate*, **19**, 2122–2143, https://doi.org/10.1175/JCLI3761.1.

Dai, Y., and Q. C. Zeng, 1997: A land surface model (IAP94) for climate studies Part I: Formulation and validation in off-line experiments. *Adv. Atmos. Sci.*, **14**, 433–460, https://doi.org/10.1007/s00376-997-0063-4.

Dai, Y. J., and Coauthors, 2003: The common land model. *Bull. Amer. Meteor. Soc.*, **84**, 1013–1024, https://doi.org/10.1175/BAMS-84-8-1013.

Dai, Y. J., R. E. Dickinson, and Y. P. Wang, 2004: A two-big-leaf model for canopy temperature, photosynthesis, and stomatal conductance. *J. Climate*, **17**, 2281–2299, https://doi.org/10.1175/1520-0442(2004)017<2281:ATMFCT>2.0.CO;2.

Dong, X., and Coauthors, 2020: CAS-ESM2.0 model datasets for the CMIP6 Ocean Model Intercomparison Project Phase 1 (OMIP1). *Adv. Atmos. Sci.*, https://doi.org/10.1007/s00376-020-0150-3.

Eyring, V., S. Bony, G. A. Meehl, C. A. Senior, B. Stevens, R. J.

Stouffer, and K. E. Taylor, 2016: Overview of the Coupled Model Intercomparison Project Phase 6 (CMIP6) experimental design and organization. *Geoscientific Model Development*, **9**, 1937–1958, https://doi.org/10.5194/gmd-9-1937-2016.

Fairall, C. W., E. F. Bradley, J. E. Hare, A. A. Grachev, and J. B. Edson, 2003: Bulk parameterization of air-sea fluxes: Updates and verification for the COARE algorithm. *J. Climate*, **16**, 571–591, https://doi.org/10.1175/1520-0442(2003)016<0571:BPOASF>2.0.CO;2.

Gregory, J. M., and Coauthors, 2005: A model intercomparison of changes in the Atlantic thermohaline circulation in response to increasing atmospheric CO_2 concentration. *Geophys. Res. Lett.*, **32**, L12703, https://doi.org/10.1029/2005GL023209.

Gregory, J. M., and Coauthors, 2016: The flux-anomaly-forced model intercomparison project (FAFMIP) contribution to CMIP6: Investigation of sea-level and ocean climate change in response to CO_2 forcing. *Geoscientific Model Development*, **9**(11), 3993–4017, https://doi.org/10.5194/gmd-9-3993-2016.

Hunke, E. C., and J. K. Dukowicz, 1997: An elastic–viscous–plastic model for sea ice dynamics. *J. Phys. Oceanogr.*, **27**, 1849–1867, https://doi.org/10.1175/1520-0485(1997)027<1849:AEVPMF>2.0.CO;2.

Hunke, E. C., and W. H. Lipscomb, 2008: CICE: The Los Alamos sea ice model user's manual, version 4. Los Alamos National Laboratory Tech. Rep. LA-CC-06-012, 76 pp.

IPCC, 2013: Sea level change. *Climate Change 2013-The Physical Science Basis. Contribution of Working Group I to the Fifth Assessment Report of the Intergovernmental Panel on Climate Change*, T. F. Stocker et al., Eds., Cambridge University Press, https://doi.org/10.1017/CBO9781107415324.026.

Ji, D., and Coauthors, 2014: Description and basic evaluation of Beijing Normal University Earth System Model (BNU-ESM) version 1. *Geoscientific Model Development*, **7**, 2039–2064, https://doi.org/10.5194/gmd-7-2039-2014.

Jin, J. B., Q. C. Zeng, L. Wu, H. L. Liu, and M. H. Zhang, 2017: Formulation of a new ocean salinity boundary condition and impact on the simulated climate of an oceanic general circulation model. *Science China Earth Sciences*, **60**, 491–500, https://doi.org/10.1007/s11430-016-9004-4.

Lipscomb, W. H., and E. C. Hunke, 2004: Modeling sea ice transport using incremental remapping. *Mon. Wea. Rev.*, **132**, 1341–1354, https://doi.org/10.1175/1520-0493(2004)132<1341:MSITUI>2.0.CO;2.

Lipscomb, W. H., E. C. Hunke, W. Maslowski, and J. Jakacki, 2007: Ridging, strength, and stability in high-resolution sea ice models. *J. Geophys. Res.*, **112**, C03S91, https://doi.org/10.1029/2005JC003355.

Liu, H. L., P. F. Lin, Y. Q. Yu, and X. H. Zhang, 2012: The baseline evaluation of LASG/IAP climate system ocean model (LICOM) version 2. *Acta Meteorologica Sinica*, **26**, 318–329, https://doi.org/10.1007/s13351-012-0305-y.

Liu, J. P., 2010: Sensitivity of sea ice and ocean simulations to sea ice salinity in a coupled global climate model. *Science China Earth Sciences*, **53**, 911–918, https://doi.org/10.1007/s11430-010-0051-x.

Rahmstorf, S., and A. Ganopolski, 1999: Long-term global warming scenarios computed with an efficient coupled climate model. *Climatic Change*, **43**, 353–367, https://doi.org/10.1023/A:1005474526406.

Stouffer, R. J., and Coauthors, 2006: Investigating the causes of the response of the thermohaline circulation to past and future climate changes. *J. Climate*, **19**, 1365–1387, https://doi.org/10.1175/JCLI3689.1.

Yin, J. J., 2012: Century to multi-century sea level rise projections from CMIP5 models. *Geophys. Res. Lett.*, **39**, L17709, https://doi.org/10.1029/2012GL052947.

Zeng, Q. C., X. H. Zhang, X. Z. Liang, C. Yuan, and S. Chen, 1989: Documentation of IAP two-level Atmospheric General Circulation Model. DOE/ER/60314-H1, TR044, 383pp.

Zeng, X. D., F. Li, and X. Song, 2014: Development of the IAP dynamic global vegetation model. *Adv. Atmos. Sci.*, **31**, 505–514, https://doi.org/10.1007/s00376-013-3155-3.

Zhang, H., and Coauthors, 2020: CAS-ESM 2: Description and climate simulation performance of the Chinese Academy of Sciences (CAS) Earth System Model (ESM) version 2. *Journal of Advances in Modeling Earth Systems*, https://doi.org/10.1029/2020MS002210.

Zhang, X. H., and Q. C. Zeng, 1988: A computational design of numerical world genera1 circulation model. *Chinese Journal of Atmospheric Sciences*, **12**, 149–165, https://doi.org/10.3878/j.issn.1006-9895.1988.t1.13. (in Chinese)

Zhou, G. Q., and Coauthors, 2020: Earth system model: CAS-ESM. *Frontiers of Data & Computing*, **2**(1), 38–54, https://doi.org/10.11871/jfdc.issn.2096-742X.2020.01.004. (in Chinese)

Zhou, T. J., L. W. Zou, and X. L. Chen, 2019: Commentary on the Coupled Model Intercomparison Project Phase 6 (CMIP6). *Climate Change Research*, **15**(5), 445–456, https://doi.org/10.12006/j.issn.1673-1719.2019.193. (in Chinese)